Available online at www.sciencedirect.com
SCIENCE DIRECT®
PERGAMON
International Journal of Multiphase Flow 29 (2003) 1431–1450
International Journal of Multiphase Flow
www.elsevier.com/locate/ijmulflow

Unsteady three-dimensional simulation of interactions between flow and two particles

T. Tsuji [a,*], R. Narutomi [a,1], T. Yokomine [b], S. Ebara [b], A. Shimizu [b]

[a] *Advanced Energy Engineering Sciences, Kyushu University, 6-1 Kasuga-koen, Kasuga, Fukuoka 816-8580, Japan*

[b] *Energy Science Division, Kyushu University, 6-1 Kasuga-koen, Kasuga, Fukuoka 816-8580, Japan*

Received 3 June 2002; received in revised form 24 June 2003

Abstract

Unsteady three-dimensional simulation of interactions between uniform flow and fixed identical two particles is performed for particle Reynolds number 30, 100, 200 and 250. The drag force of interactive particles depends on Reynolds number as well as the inter-particle distance. They are attenuated when particles are aligned streamwise, augmented when they are held side by side against the mean flow. These are compared with available experimental data. Existence of periodical double-sided vortex shedding at relatively low Reynolds number is observed when particles are almost touching. The method adopted in this paper is not only simple and easy, but also accurate with a proper resolution.

Keywords: Flow–particles interaction; Multiphase flow; Direct numerical simulation; Drag force; Visualization; Wake structure

1. Introduction

Particulate multiphase flow that carries small particles or droplets in flow is quite important in natural and industrial fields such as diffusion of pollutant, energy conversion systems, combustion systems, and chemical processes. In this kind of flow, transportation of momentum,

* Corresponding author. Tel.: +81-92-583-7603; fax: +81-92-583-7601.
E-mail address: tsuji@aees.kyushu-u.ac.jp (T. Tsuji).
URL: http://phase.ence.kyushu-u.ac.jp/~tak/.
[1] Present address: Mitsubishi Heavy Industries Co. Ltd., Tokyo, Japan.

0301-9322/$ - see front matter
doi:10.1016/S0301-9322(03)00137-X

mass, and heat through phases characterizes the flow. When particle concentrations come up to a certain level, the arrangement of particles becomes an important factor to determine the flow characteristics. Systematized particles may act as turbulence accelerators in some cases, and act as the flow blockade to result in increase of pressure drop in others. Toward the efficient and accurate controlling and modeling of the particulate multiphase flow, clarification of fluid dynamic mechanism at high particle concentration is desired. Of course, this is not easy, when the particle concentration increases, the flow becomes quite complex and this comes to be the subject of uncertainly. It is necessary to accumulate the fundamental information that take place locally one by one. Interactions between particles and flow at intermediate particle Reynolds number Re (based on particle terminal velocity, diameter and fluid viscosity) are not known well, even if the number of particle is two. Early experimental works are carried by Rowe and Henwood (1961), Lee (1979), and Tsuji et al. (1982) focused on the effect of an inter-particle distance on the flow characteristics for $Re > 200$. However, they could not give quantitative results due to the accuracy of measurements. Zhu et al. (1994) measured the drag of two interactive particles arranged in the longitudinal direction for $Re < 200$ using an electronic balance and conducted the flow visualization. They concluded that the drag force on an interactive sphere highly depend on the wake structure. Though a study of larger number of particle more than two was done by Liang et al. (1996), no explanations of the wake flow structure relating to the change of drag forces were presented. Recently, Chen and Lu (1999) and Chen and Wu (2000) measured both the drag and the wake structure of an interactive particle, simultaneously, and physical interpretations were given. However, number of particle in their studies was still limited to three. All of this amounts to saying that quantitative measurement of the flow field with large number of particles in complex arrangement is quite difficult based on the current measurement techniques, i.e. LDV, PIV. Therefore, numerical simulation may be the left and the only way at current situation to investigate the mechanism. However, numerical study of interactions between flow and particles is limited. Kim et al. (1993) simulated the interactions between flow and two spheres held fixed side by side against the uniform upstream at Re numbers 50, 100, and 150, where generalized coordinates were used with the assumption of symmetry of flow. Same configuration was computed by Folkersma et al. (2000) for $Re = 5 \times 10^{-7}$, 10, 50 by finite element method. Number of particle was limited to two in these studies. Liang et al. (1996) studied the flow around three particles aligns streamwise at $Re < 110$. They also used finite element method, and axisymmetry of flow was assumed. Not only these previous numerical studies were limited to $Re < 150$, but some symmetries and steadiness conditions of flow were assumed to reduce the computational costs. When the particle concentration and Re number increase, it is supposed that interactions with the surrounding particle may destroy the symmetry of flow, and flow field may have real three-dimensional features. Accordingly, the methods stand on the symmetries and steadiness conditions of flow cannot be extended to the simulation of further number of particle in complex arrangement. Unsteady three-dimensional approach with less computational load is required. In this paper, as a first step towards the understanding of the interactions in large concentration of particles, we conduct the unsteady three-dimensional numerical simulation of interactions between uniform flow and fixed identical two particles for $Re = 30$, 100, 200, and 250. Typical two particle arrangements are adopted. One is on the line parallel to the mean flow direction and the other is placed side by side to it. Relations between particle positions and flow characteristics are verified in detail from our calculation and visualization results.

2. Simulation method

2.1. Governing equations

Assuming that the fluid of interest is viscous and incompressible, and particle is rigid and fixed. The governing equations of flow are continuity and Navier–Stokes equations:

$$\nabla \cdot \boldsymbol{u}_{\mathrm{f}} = 0, \tag{1}$$

$$\rho_{\mathrm{f}} \frac{\mathrm{D}\boldsymbol{u}_{\mathrm{f}}}{\mathrm{D}t} = \nabla \cdot \boldsymbol{\tau} + \rho_{\mathrm{f}} \boldsymbol{g}, \tag{2}$$

where ρ_{f} denotes the fluid density, $\boldsymbol{u}_{\mathrm{f}}$ the fluid velocity, $\boldsymbol{\tau}$ the stress tensor:

$$\boldsymbol{\tau} = -p\boldsymbol{I} + \mu_{\mathrm{f}}[\nabla \boldsymbol{u}_{\mathrm{f}} + (\nabla \boldsymbol{u}_{\mathrm{f}})^{\mathrm{T}}], \tag{3}$$

p the static pressure, μ_{f} the fluid viscosity. ρ_{f} and μ_{f} are assumed to constant in our study. The last term of the right-hand of Eq. (2) is external force such as gravity.

2.2. Coupling method using particle volume fraction

This study is the first period of continuous work towards the understanding of interaction mechanism between particles and surrounding flow. In such flows, of course particles are allowed to move, rotate and collide with other particles and walls. Hence, a scheme which can treat these features should be adopted taking the future extension of study into account while particles are fixed in present study. A number of methods exist for this type of simulation. And these can be classified into two groups in general. One is moving grid type where grid points move corresponding to the change of flow field. Hu (1996) has developed an arbitrary Eulerian–Lagragian (ALE) scheme based on finite elements and unstructured grids to compute the motion of several moving particles in a flow. Similar schemes, i.e. Johnson and Tezduyar (1997) also exist. Antaki et al. (2000) have simulated the interaction of cells in blood flow by tracking the fluid elements in Lagragian way and remeshing by parallel Delaunay algorithm at each time. These are very challenging because generation of high quality mesh adjusting to moving particles in complex arrangement (especially in three-dimensions) is not trivial. What we want to investigate in this continuous work is a case where wake induced by particles interacts with background turbulence. So far as we know, however, application of this calss of scheme is resticted to laminar and particle wake-induced turbulent flow at most (background flow is laminar). On the other hand, if all computations are performed on fixed grid, this is very attractive. Pan and Banerjee (1997) performed DNS of fluid–particle interactions in turbulent flow by adding source term that models the no-slip boundary condition on the surface of the particles to governing equations. Glowinski et al. (1999) and Patankar et al. (2000) use a distributed Lagrange multiplier scheme to compute flows with multiple spherical particles. In these fixed grid schemes, faster solver can be used and extension to the three-dimensions and turbulence flow is relative easier. Our study stands on one of fixed grid schemes proposed by Kajishima et al. (2001).

Kajishima et al. (2001) developed a coupling method for moving particle–fluid system using following particle volume-weighted velocity $\boldsymbol{u}$,

$$\boldsymbol{u} = \alpha \boldsymbol{u}_\mathrm{p} + (1-\alpha)\boldsymbol{u}_\mathrm{f}, \tag{4}$$

where α is the volumetric fraction of particle at the targeted cell, $\boldsymbol{u}_\mathrm{p}$ is the velocity inside of particle. Present study stands on the same idea while particle is fixed. Hence, letting $\boldsymbol{u}_\mathrm{p} = 0$, Eq. (4) becomes

$$\boldsymbol{u} = (1-\alpha)\boldsymbol{u}_\mathrm{f}. \tag{5}$$

No-slip and no-permeable conditions are imposed on its interface because particle is rigid. Thus the continuity restriction is also assured on $\boldsymbol{u}$,

$$\nabla \cdot \boldsymbol{u} = 0. \tag{6}$$

Equation for $\boldsymbol{u}$ is introduced.

$$\frac{\partial \boldsymbol{u}}{\partial t} = -\frac{1}{\rho_\mathrm{f}}\nabla p + \boldsymbol{H} + \boldsymbol{f}_\mathrm{p}, \tag{7}$$

where

$$\boldsymbol{H} = -\boldsymbol{u}\cdot\nabla\boldsymbol{u} + \nu_\mathrm{f}\nabla\cdot[\nabla\boldsymbol{u} + (\boldsymbol{u}^\mathrm{T})] + \boldsymbol{g}, \tag{8}$$

and ν_f is the kinematic viscosity of fluid. The formation of the Eq. (8) similar to the Navier–Stokes equation (Eq. (2)) except for the last term. $\boldsymbol{f}_\mathrm{p}$ is the force to modify the flow predicted as if the field is occupied by fluid to the velocity defined by Eq. (4). This is explained in terms of time-marching procedure. If Eq. (7) march in time with explicit Euler method, this may be

$$\boldsymbol{u}^{n+1} = \boldsymbol{u}^n + \Delta t\left(-\frac{1}{\rho_\mathrm{f}}\nabla p + \boldsymbol{H} + \boldsymbol{f}_\mathrm{p}\right), \tag{9}$$

where superscript represents time, and Δt the time increment. We predict the velocity as the fluid phase once, $\tilde{\boldsymbol{u}} = \boldsymbol{u}^n + \Delta t(-1/\rho\nabla p + \boldsymbol{H})$, despite what is in the targeted cell, fluid ($\alpha = 0$), particle ($\alpha = 1$), both ($0 < \alpha < 1$). The predicted velocity should be modified by $\boldsymbol{f}_\mathrm{p}$ to meet the definition of $\boldsymbol{u}^{n+1}$. For the cell inside of the particle ($\alpha = 1$), $\boldsymbol{f}_\mathrm{p} = -\tilde{\boldsymbol{u}}/\Delta t$ gives $\boldsymbol{u}^{n+1} = 0$ (inside of particle). For the cell occupied with fluid ($\alpha = 0$), on the other hand, Eq. (7) is identical to Eq. (2) because $\boldsymbol{f}_\mathrm{p}$ vanishes. Hence, added term $\boldsymbol{f}_\mathrm{p}$ is modeled with linear interpolation of α

$$\boldsymbol{f}_\mathrm{p} = -\alpha\tilde{\boldsymbol{u}}/\Delta t. \tag{10}$$

This is a force to modify the solution of Eq. (7) to the particle volume-weighted velocity $\boldsymbol{u}$. And this is interpreted as the momentum exchange through interface.

2.3. Computational scheme

Spatial derivatives are discritized using fourth order central difference method. Time-marching are based on the fractional step method with second order Adams–Bashforth scheme. The time-marching procedure is as follows.

(1) The fractional step velocity of Eq. (7) without pressure term is obtained.

$$\tilde{\boldsymbol{u}} = \boldsymbol{u}^n + \frac{\Delta t}{2}(3\boldsymbol{H}^n - \boldsymbol{H}^{n-1}). \tag{11}$$

(2) Poisson equation for the scalar potential ϕ is solved by SOR (successive over relaxation) method.

$$\nabla^2\phi^{n+1} = \frac{1}{\Delta t}\nabla\tilde{\boldsymbol{u}}. \tag{12}$$

(3) Velocity $\tilde{\boldsymbol{u}}$ is updated with scalar potential ϕ^{n+1}, existence of particle can be neglect until this step.

$$\hat{\boldsymbol{u}} = \tilde{\boldsymbol{u}} - \Delta t\nabla\phi^{n+1}. \tag{13}$$

(4) Evaluating the interaction force.

$$\boldsymbol{f}_{\mathrm{p}} = -\frac{\alpha}{\Delta t}\hat{\boldsymbol{u}} \tag{14}$$

and update the velocity obtained in step 3.

$$\boldsymbol{u}^{n+1} = \hat{\boldsymbol{u}} + \Delta t\boldsymbol{f}_{\mathrm{p}}. \tag{15}$$

Pressure is calculated by the following relation:

$$p^{n+1} = \phi^{n+1} - \frac{\nu_{\mathrm{f}}}{2}\Delta t\nabla^2\phi^{n+1}. \tag{16}$$

In this way, time-marching for Eqs. (6) and (7) is finished.

2.4. Volumetric fraction of particle by subdivision volume counting method

Evaluation of the particle volumetric fraction α is crucial in this method. This can be measured exactly when geometrical configurations such as a shape of surface and a position relative to the grid are given. But this is very time consuming in three-dimensional computation. Kajishima et al. (2001) reduced it by approximating the surface of particle by tangential planes normal to the relative vector from the center of particle to a center of interfacial cells. This is shown in Fig. 1. We denote it as TP method in this paper. Although TP method decreases the computation time, it still requires further improvements. In three-dimensional space computation, it is not so easy to generate the tangential planes at each interfacial cells. Besides, when the number of particle increases, it is expected that it still occupy significant part of total computation time. Another problem is that TP method inherently overestimates the particle volume. To solve the shortcoming of TP method, we propose a new method named "subdivision volume counting (SVC)" as

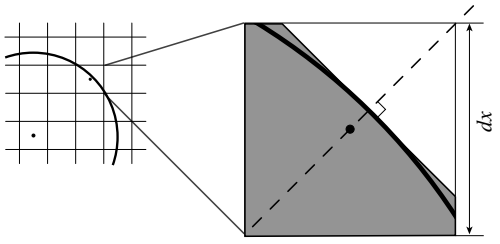

Fig. 1. Tangential plane approximation by Kajishima et al. (2001).

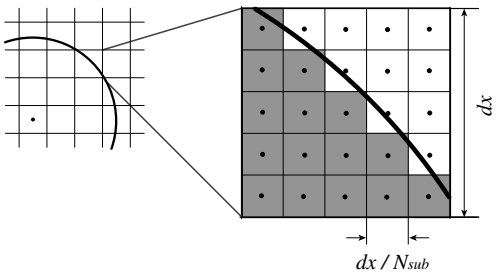

Fig. 2. Proposed subdivision volume counting method.

an alternative. In this method, each interfacial cells are subdivided into small elements. If the length between the center of particle and element is shorter than the particle diameter, the volume of the element is counted as particle in this cell. This is demonstrated in Fig. 2. We obtain the particle volume fraction of one cell after evaluating each subdivided elements.

$$\alpha = \frac{\text{Number of elements } (l \leqslant d) \text{ at the cell}}{\text{Total number of elements at the cell}}, \tag{17}$$

where l denotes distance between the center of particle and cell. Applying this procedure at all interfacial cells sequentially, we obtain all α that is needed to calculate the interaction force.

3. Preliminary computations

3.1. Evaluation of subdivision volume counting method

Performance of the SVC method was verified first. This test was performed in two-dimensional. Thus, cell is subdivided into square planes. Number of subdivision for each direction is defined as N_{sub}. $N_{\text{sub}} = 10$, 5 was selected as test cases. Fig. 3 shows relations between resolution of computation and approximated area, where the resolution is defined as ratio between particle diameter d and uniform mesh width dx. We can confirm that the SVC approximates better than the

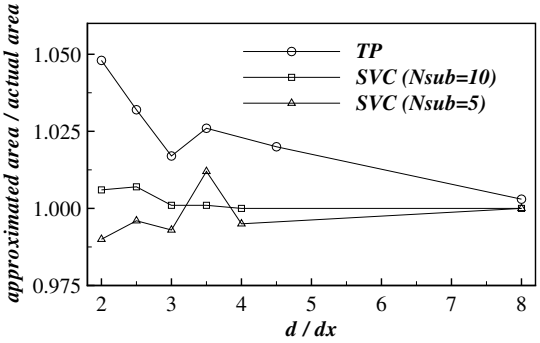

Fig. 3. Subdivision volume counting method vs. tangential plane approximation method.

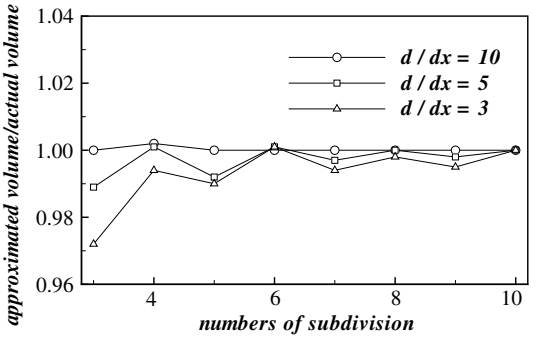

Fig. 4. Number of subdivision and resolution of computation.

TP generally from Fig. 3. Error of SVC method is under 1% even for $d/dx = 2$, $N_{sub} = 5$. In addition to accuracy, the SVC method holds another important advantages. First, this method is highly simple and easy to write a code because we are just measuring the distance between the center of particle and each element. Second, it may requires lower computation time comparing to the TP method. Third, it does not require excessive memory because subdivision of cell is performed sequentially. It can be said that all of these features of SVC method are superior to TP method.

Fig. 4 shows the relation between the number of subdivision and approximated volume of particle. The approximation improves with increase in N_{sub}. But excessive number of subdivision just leads to unnecessary computational loads. An optimal number of subdivision is verified here. We can confirm from Fig. 4 that error is just 3% even if the case $N_{sub} = 3$, $d/dx = 3$, this is the coarsest case in our preliminary computation. The error becomes under 1% at $N_{sub} \geqslant 6$. Hence, $N_{sub} = 6$ is adopted for all computation hereafter.

3.2. Optimal domain size and resolutions

A series of preliminary computations was carried out in order to determine the optimal resolution and domain size. Determination of optimal value is important because we adopt uniform staggered grid in Cartesian coordinates. We set x, y, z for the vertical, lateral, streamwise (longitudinal) direction, respectively. Numbers of grid point for each direction are defined as N_x, N_y, and N_z, respectively. Working fluid is assumed to air at standard condition ($\mu_f = 1.784 \times 10^{-5}$ Pa s, $\rho_f = 1.226$ kg/m^3). Uniform mesh width dx is set to 1×10^{-3} m. Time increment is set to $dt = 1 \times 10^{-3}$ s. A uniform velocity was imposed as the inflow boundary condition. Desired Re number is obtained by adjusting the upstream uniform velocity. A primary function of side and outflow boundary conditions in a numerical simulation are to allow the flow variables to leave the computational domain without perturbing inside of the calculation domain. Hence, a traction-free and a convective boundary condition is imposed on the side boundaries and outflow boundary, respectively. To avoid the numerical instability at earlier time stage of calculation, all components of initial velocity are set to zero and uniform upstream velocity is given gradually. Initial pressure is set to the standard atmosphere.

Table 1
Drag coefficients with different resolutions at $Re = 300$

d/dx	8	16	24	White (1974)	Morsi and Alexander (1972)
C_d	0.907	0.729	0.714	0.808	0.661

First, grid resolution was checked. Flow around single particle at $Re = 300$ is selected as the test case. The particle is located at the origin of coordinates. At such Re number, it is expected that the detached flow from the particle surface form the periodic structures well known as the hairpin vortex. Drag coefficients at different resolutions ($d/dx = 8$, 16, 24) were compared in Table 1.

Ordinary, fluid force acting on the particle is evaluated by performing the surface integral of fluid stress on the particle surface. But this can be replaced by the volume integral of interaction force $\boldsymbol{f}_p$, thus

$$\boldsymbol{F} = \rho_f \int_{V_p} \boldsymbol{f}_p \, dV + \boldsymbol{G}_p, \tag{18}$$

where $\boldsymbol{F}$ is fluid force acting on the particle, V_p the particle volume, and $\boldsymbol{G}_p$ the external force. Drag coefficient C_d is defined as

$$C_d = \frac{F_z}{\frac{1}{8}\rho_f U_0^2 d^2}, \tag{19}$$

where U_0 is the upstream uniform velocity, F_z is the streamwise fluid force acting on the particle. The drag coefficient was time-averaged after steady state had reached. Domain size is set to $N_x \times N_y \times N_z = 100 \times 100 \times 200$. We took 40 grids as the upstream region from the inflow boundary to the center of particle because difference of drag coefficient between a case of 40 and 100 grids was almost 1%. At $d/dx = 8$, the result is almost 25% larger than the standard curve by White (1974). As increases the resolution, drag coefficient approaches to the value between White (1974) and Morsi and Alexander (1972). Difference between $d/dx = 16$ and $d/dx = 24$ is just 2%, and it seems to be almost converged. Accordingly, we adopt $d/dx = 16$ for all computations hereafter.

Second, optimal domain size was investigated. Flow around the single particle at $Re = 100$ was selected as the test case. The result with various cross section size $N_x = N_y = 64$, 80, and 100 is shown in Table 2.

Table 2
Drag coefficients of various domain size at $Re = 100$

Cases	$N_x(= N_y)$	C_d
Present	64	1.16
Present	80	1.17
Present	100	1.18
White (1974)	Experiment	1.18

Difference between $N_x = N_y = 64$ and $N_x = N_y = 100$ is just 1.5%. The case $N_x = N_y = 100$ agreed with White (1974) very well. Hence, we adopted $N_x = N_y = 100$.

4. Results and discussion

4.1. Drag on single particle

Drag coefficients of isolated particle with various *Re* numbers $Re = 1$, 10, 30, 100, 200, 250, 280, and 300 are shown in Fig. 5. Drag coefficients generally agree with the literature. In recent study, Patankar (2001) pointed out the limitation of this scheme such as first-order accuracy in time and the numerical stability. These problems become problematic if we take large time increment, but in present study, it was set to $dt = 1 \times 10^{-3}$ s, and corresponding Courant number is less than 0.2. It requires longer computational time but, in such condition, any problem could not be observed at all. Further studies are needed for the improvement of efficiency. In our calculation, separated wake keeps axisymmetry at $1 < Re < 200$ and plane symmetry until $Re = 250$, starts to shed and become unsteady at $Re = 280$. This trend of transition almost agree with the calculation by Johnson and Patel (1999).

4.2. Two particles aligned streamwise

Two particles placed aligning streamwise was investigated. Drag coefficient of leading (upstream) and trailing (downstream) particle are defined as C_{d1} and C_{d2}, respectively. Calculation condition is same as the preliminary computation. The origin of axes is set to the center of leading particle. Fig. 6 is the relation between the drag coefficient of the leading particle and the inter-particle distance. Drag coefficient is non-dimensionalized by a drag coefficient of single particle under the same *Re* number. Inter-particle distance l is defined as a distance between particle surfaces, and this is also expressed in a dimensionless form l/d. Slight attenuation of drag force

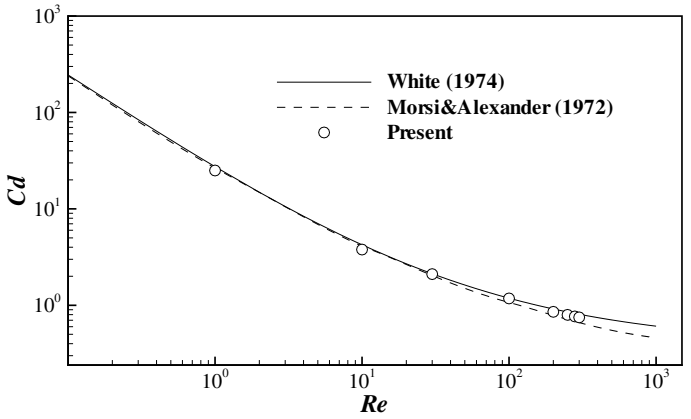

Fig. 5. Drag coefficients of single particle.

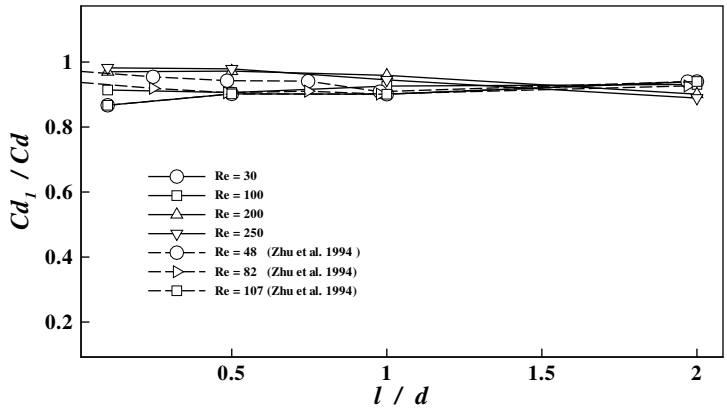

Fig. 6. Drag coefficients of leading particle for two particles aligned streamwise.

can be confirmed for all Re and l/d. But, Reynolds number dependency is not significant. This is almost in agreement with the experimental results by Zhu et al. (1994). When particles aligned streamwise, the lower pressure region behind leading particle is interfered by the high pressure region exists in front of the trailing particle. This is demonstrated in Fig. 7(b)–(d). For comparison, pressure coefficients distribution around the single particle is also shown in Fig. 7(a). C_p is pressure coefficient defined as

$$C_p = \frac{p - p_\infty}{\frac{1}{2}\rho_f U_0^2}, \tag{20}$$

where p_∞ is set to the standard atmospheric pressure. At $l/d = 0.1$, 0.5 (Fig. 7(b) and (c)), it seemed that the trailing particle is captured by the lower pressure region behind the leading particle. As it increases to $l/d = 2$ (Fig. 7(d)), it seemed that the trailing particle is escaped from the lower pressure region. But higher pressure region which expect to occur in front of the trailing particle like Fig. 7(a) does not exist by the influence of the leading particle. These pressure interferes relax the streamwise pressure gradient, and results in the reduction of form drag.

Fig. 8 is the drag coefficients of the trailing particle. Attenuation of the drag force by the influence of leading particle is clearly observed. Especially, for $Re = 250$, $l/d = 0.1$, the drag force is reduced to almost 7% of the single particle. Form drag of the trailing particle were attenuated by the pressure interferences with the leading particle. But, at such Re number, it is expected that the form drag occupies a small part of the total drag. Large attenuation may be caused primarily by the reduction of friction drag. Separated flow from the leading particle did not swallow the trailing particle, but it is suppressed and makes ring-like vortices region between particles. This is depicted in Fig. 9 for $Re = 200$, $l/d = 0.5$. Corresponding kinetic energy distribution and vector map are shown in Figs. 10 and 11, respectively. It seems that fluid is moving in a relative slow manner, and this ring-like vortices is isolated from the main stream at this region. As l/d increases, this ring-like vortices are stretched for streamwise. This is demonstrated in Fig. 12. These nearly stagnant and slow moving vortical flow between particles decrease the friction drag of the trailing particle significantly, and result in the large attenuation of total drag. These observations are agreed with experiments by Zhu et al. (1994) and Chen and Lu (1999). They also reported a

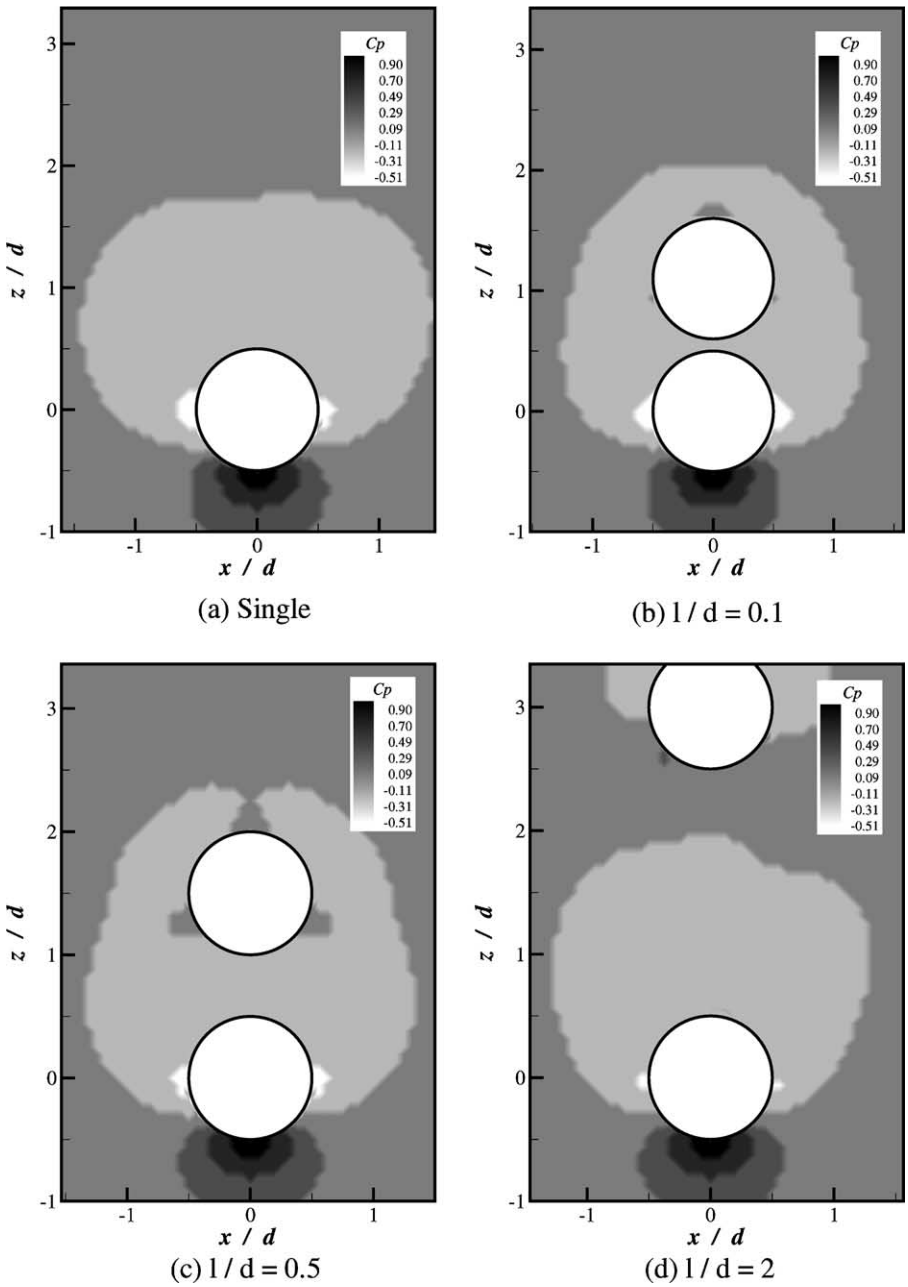

Fig. 7. Pressure coefficients distributions of inter-particle region on $y = 0$ lateral plane for $Re = 250$.

drag force dependency on *Re* number, but their results were not so significant. In our calculation, on the other hand, this is clearly observed from Fig. 8. Drag force of the trailing particle decreases with an increase in *Re*. This trend can be explained by above mentioned reasons.

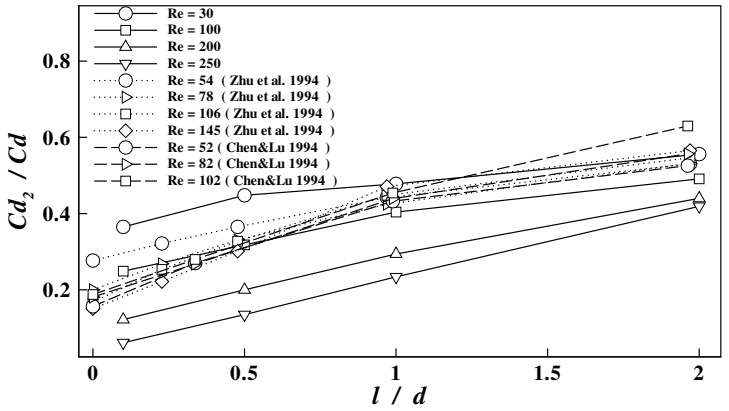

Fig. 8. Drag coefficients of trailing particle for two particles aligned streamwise.

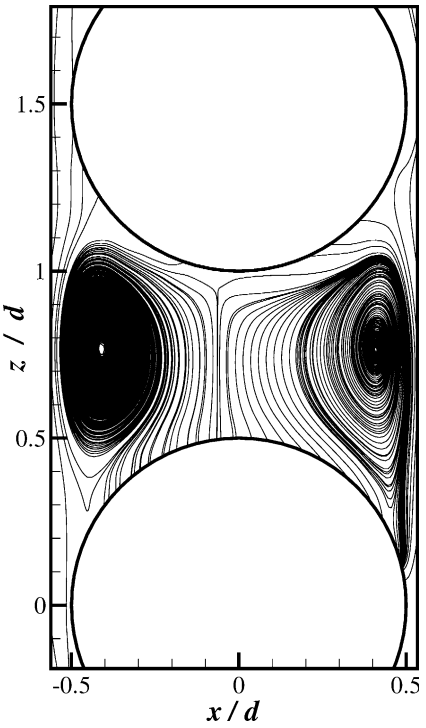

Fig. 9. Streamline of inter-particle region on $y = 0$ lateral plane for two particles aligned streamwise at $Re = 200$, $l/d = 0.5$.

Our results shows characteristics on transition in case of two particles aligned streamwise. Vortical structure behind trailing particle keeps axisymmetry in all cases we performed (even

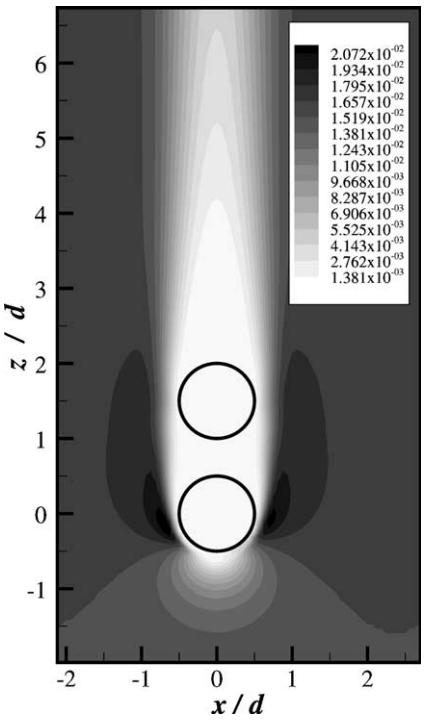

Fig. 10. Kinetic energy on $y = 0$ lateral plane for two particles aligned streamwise at $Re = 200$, $l/d = 0.5$.

$Re = 250$) while it breaks and shifts off-axis at $Re = 210$ in single particle case (Johnson and Patel, 1999). In addition, if particle distance is small ($l/d = 0.1$, 0.5), vortex behind leading particle (in between two particles), does not shift off-axis and keeps axisymmetry in $Re = 250$ case. We could not observe the onset of vortex shedding from our limited cases. However, we can say that, when particles are arranged in streamwise and especially if particle distance is small, starts of transition are delayed comparing to the single particle case.

4.3. Two particles aligned side by side

Next, we investigated the two particles held fixed side by side toward the main flow direction. Two particles are placed on the line parallel to x (vertical) direction. The midpoint between the center of particles is set to the origin of x axis, The origins of other axes are set to the center of particles, respectively. Calculation condition is that of preliminary computation except for the length of vertical direction. This is extended to $N_x = 150$ in case of $l/d = 2$. As we expected, differences of the drag force between two particles are not significant. Hence, results of one particle are shown here. Fig. 13 is the relation between drag coefficient and inter-particle distance. Slight attenuation of drag force can be confirmed for all Re and l/d. As l/d decreases, the drag force increases except for $Re = 30$ ($l/d < 0.5$). Similar trend can be seen in the previous experiments (Chen and Lu, 1999) and especially it agree with computational results by Kim et al. (1993) for the low Re number case. Pressure coefficients distribution at $Re = 200$, $l/d = 0.1$ is shown in

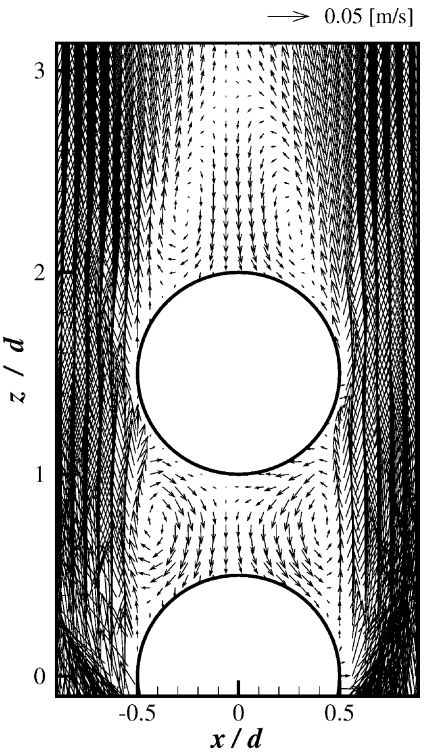

Fig. 11. Velocity vectors on $y = 0$ lateral plane for two particles aligned streamwise at $Re = 200$, $l/d = 0.5$.

Fig. 14. Higher pressure regions that occurs in front of each particle unite each other and form a larger region. So do lower region in the behind of particle. It is better to say that the pressure region are formed around a bigger connected body. These augment the streamwise pressure gradient. Streamwise pressure gradient becomes significant when inter-particle distance becomes smaller. At lower *Re* number, the form drag occupies a small part of total drag. This is considered as the answer for that drag coefficient of $Re = 30$ does not become maximum at $l/d = 0.1$. And for $l/d = 0.5$, 1, and 2, other factor which augment the drag exists. Fig. 15(a)–(d) shows the kinetic energy variations with l/d for $Re = 200$. At $l/d = 0.5$, 1 (Fig. 15(b) and (c)), high kinetic energy region between particles is observed. This is so-called "nozzle effect". The nozzle effect increases local *Re* numbers because flow try to pass through the small gap between particles. Consequently, the friction drag is augmented through the increase in the velocity gradient near the particle surface. At $l/d = 2$ (Fig. 15(d)), the nozzle effect almost disappeared, and the drag augmentation by the nozzle effect tend to be relaxed. *Re* number dependency of drag force is clearly observed in side by side arrangement, too. An increase in *Re* augments the drag force. This tendency correspond to above explanations by the pressure region enlargement and the nozzle effect.

4.4. Wake structures and transitions of two particles aligned side by side

Wake structure visualization is conducted by the method proposed by Tanaka and Kida (1993). $\nabla^2 p = 10$ iso-surfaces of $l/d = 1$, 0.5, 0.1 for $Re = 200$ are shown in Figs. 16–18,

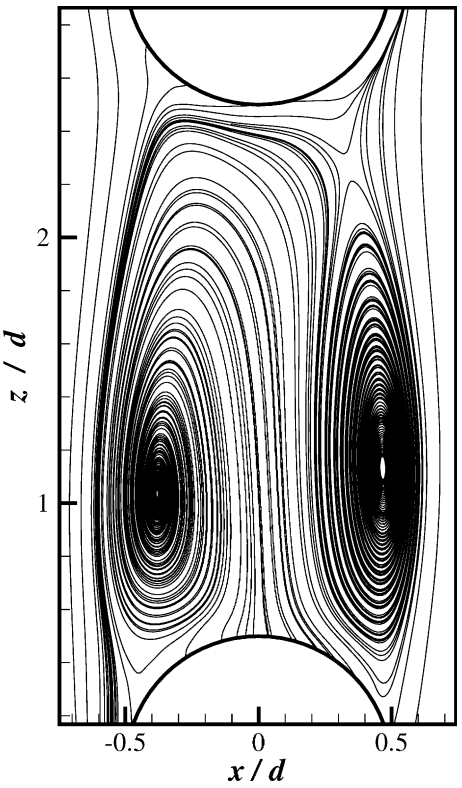

Fig. 12. Streamline of inter-particle region on $y = 0$ lateral plane for two particles aligned streamwise at $Re = 200$, $l/d = 2$.

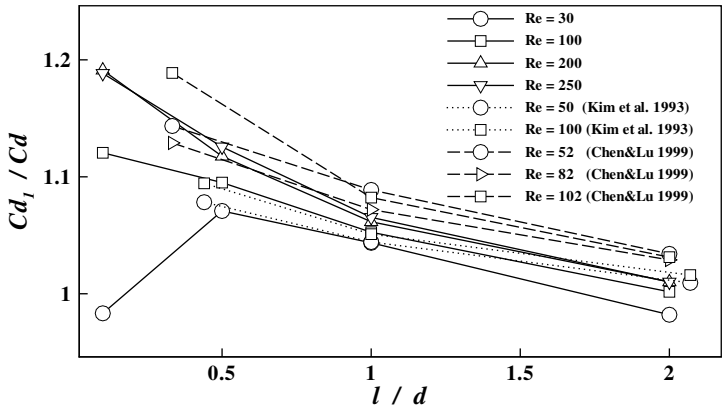

Fig. 13. Drag coefficients of one of particles aligned side by side.

respectively. Note that, in these figures, x, y, z only means the direction of coordinates for better understanding. In case of the single particle at the same Re number, separated wake keeps

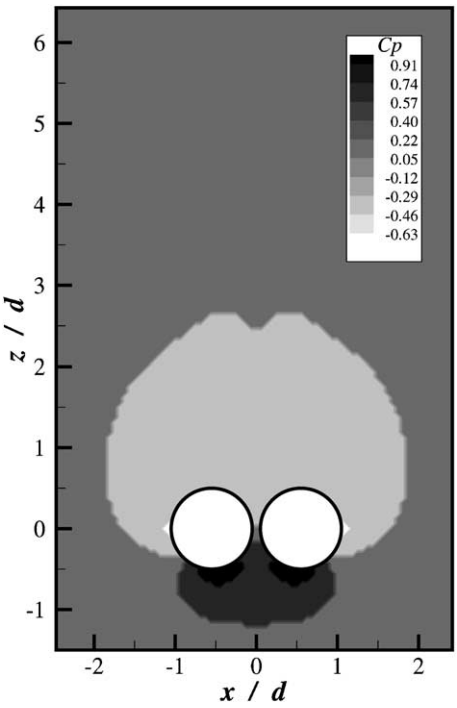

Fig. 14. Pressure coefficients distributions on $y = 0$ lateral plane for two particles aligned side by side at $Re = 200$, $l/d = 0.1$.

axisymmetry. At $l/d = 0.5$, 1 (Figs. 16 and 17), separated wake is attracted toward the center between the particles and stretched in streamwise direction. This is due to an entrainment caused by the aforementioned nozzle effect at small gap between particles. Similar trend, attraction to the center of two particles, was observed in lower *Re* number cases ($Re = 100$, 30) while they were not separated. What is most interesting is the case of $l/d = 0.1$ shown in Fig. 18. When two particles are almost touching ($l/d = 0.1$), periodical shedding of vortices which keeps symmetry on the $x = 0$ y–z plane is observed. Besides, shed wake is very stable forming double-sided structure. It resemble to the wake shedding from the single particle at first glance, but shedding mechanism is completely different. Chen and Lu (1999) reported the existence of minor swinging motion of particle at $l/d = 0$. And this motion made measurement impossible at this l/d. From our visualization results, we suppose that this is due to the periodic vortex shedding we reported here. When the vortex shedding starts, drag force may be attenuated. However, it sounds strange indeed but the drag becomes maximum at $l/d = 0.1$, $Re = 200$. Further investigation is needed. We did not attempt to further narrow the range of the onset of unsteadiness. However, from our finite numbers of computation, it is confirmed that transition occurs in the range from $Re = 100$ to 200 without reference to the particle distances l/d. Faster transition comparing to the single particle case is one of main feature of the side by side arrangement case. It is interesting that the shedding vortex shows significant difference depend on the particle distance l/d as we saw in Figs. 16–18 even *Re* number is same.

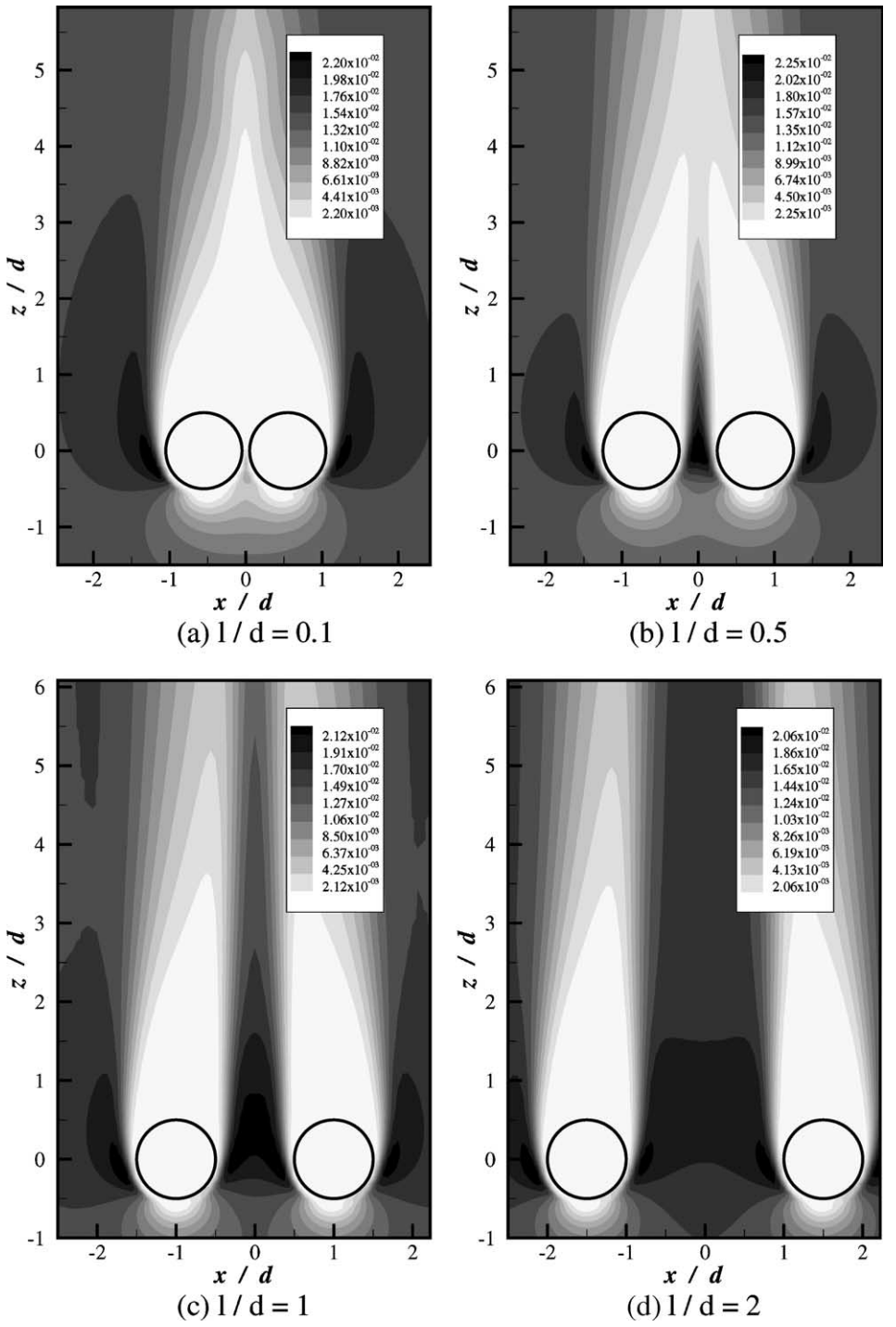

Fig. 15. Kinetic energy on $y = 0$ lateral plane for two particles aligned side by side at $Re = 200$.

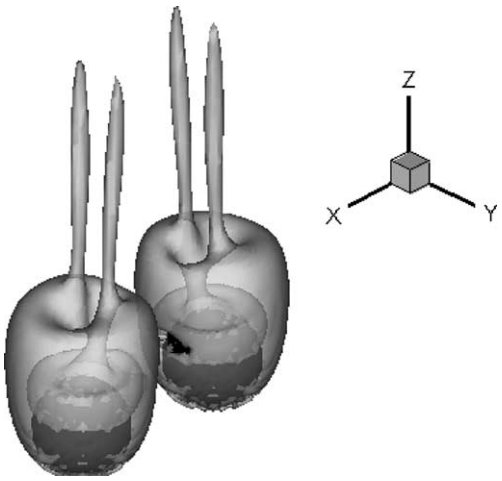

Fig. 16. $\nabla^2 p = 10$ iso-surface for two particles aligned side by side at $Re = 200$, $l/d = 1$.

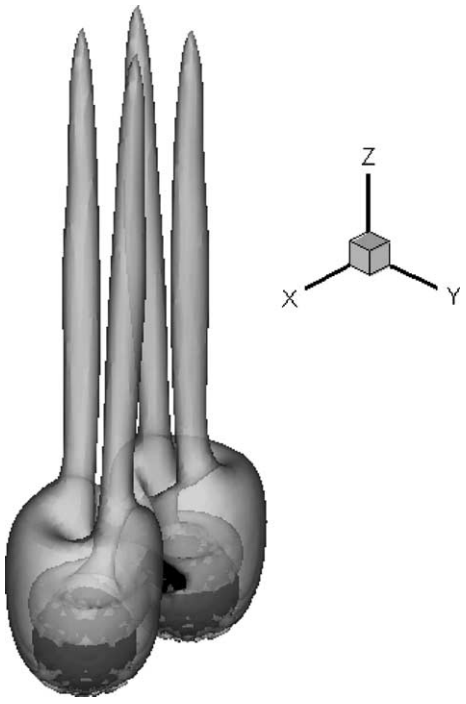

Fig. 17. $\nabla^2 p = 10$ iso-surface for two particles aligned side by side at $Re = 200$, $l/d = 0.5$.

5. Conclusion remarks

Unsteady three-dimensional numerical simulation of interactions between uniform flow and two identical particles was performed. All computations were in fixed uniform rectangular grid. From our calculation and visualization, we obtained the following conclusions.

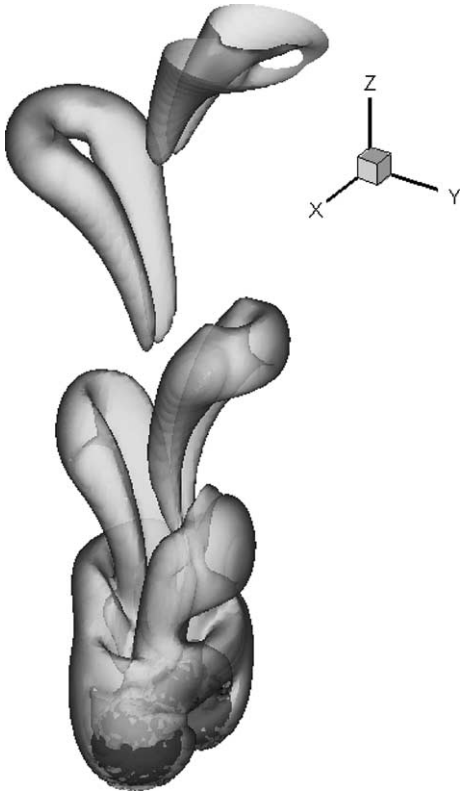

Fig. 18. $\nabla^2 p = 10$ iso-surface for two particles aligned side by side at $Re = 200$, $l/d = 0.1$.

When particles are aligned streamwise, drag forces of both particles are attenuated. Influence from the leading particle to the trailing is stronger than that from trailing to leading. Drag force of trailing particle became almost 7% of single particle at same Re number for $Re = 250$, $l/d = 0.1$. In case of particles aligned side by side to the main flow direction, drag force of both particles are augmented. This is due to the two main factors. One is the union and enlargement effect of pressure region around particles. The other is increase of the velocity gradient near the particle surface by nozzle effects. When particles are almost touching, periodical and double-sided vortex shedding exists at relatively low Re number. Drag force of interactive particles is clearly affected by Re number in both arrangements.

The method we adopted in this study is not only very simple and easy, but accurate with a proper resolution. Extension to the further number of particle in complex arrangement is fairly easy even if the particle movement is allowed. In practical system, it is important to investigate the interaction between moving particles and turbulent flow. This work is currently underway.

References

Antaki, J.F., Blelloch, G.E., Ghattas, O., Malcevic, I., Miller, G.L., Walkington, N.J., 2000. A parallel dynamic-mesh Lagrangian method for simulation of flows with dynamic interfaces. In: Proceedings of SC2000, pp. 1–11.

Chen, R.C., Lu, Y.N., 1999. The flow characteristics of an interactive particle at low Reynolds numbers. Int. J. Multiphase Flow 25, 1645–1655.

Chen, R.C., Wu, J.L., 2000. The flow characteristics between two interactive spheres. Chem. Engng. Sci. 55, 1143–1158.

Folkersma, R., Stein, H.N., Vosse, F.N., 2000. Hydrodynamic interactions between two identical spheres held fixed side by side against a uniform stream directed perpendicular to the line connecting the spheres' centres. Int. J. Multiphase Flow 26, 877–887.

Glowinski, R., Pan, T.-W., Hesla, T.I., Joseph, D.D., 1999. A distributed Lagrange multiplier/fictitious domain method for particulate flows. Int. J. Multiphase Flow 25, 755–794.

Hu, H.H., 1996. Direct simulation of flows of solid–liquid mixtures. Int. J. Multiphase Flow 22, 335–352.

Johnson, T.A., Patel, V.C., 1999. Flow past a sphere up to a Reynolds number of 300. J. Fluid Mech. 378, 19–70.

Johnson, A., Tezduyar, T., 1997. 3d simulation of fluid–particle interactions with the number of particles reaching 100. Comput. Methods Appl. Mech. Engng. 145, 301–321.

Kajishima, T., Takiguchi, S., Hamasaki, H., Miyake, Y., 2001. Turbulence structure of particle-laden flow in a vertical plane channel due to vortex shedding. JSME Int. B 44, 526–535.

Kim, I., Elbgobashi, S., Sirignano, W.A., 1993. Three-dimensional flow over two spheres placed side by side. J. Fluid Mech. 246, 465–488.

Lee, K.C., 1979. Aerodynamic interaction between two spheres at Reynolds numbers around 10^4. Aero. Q. 30, 371–385.

Liang, S.-C., Hong, T., Fan, L.-S., 1996. Effects of particle arrangements on the drag force of a particle in the intermediate flow regime. Int. J. Multiphase Flow 22, 285–306.

Morsi, S.A., Alexander, A.J., 1972. An investigation of particle trajectories in two-phase flow systems. J. Fluid Mech. 55, 193–208.

Pan, Y., Banerjee, S., 1997. Numerical investigation of the effect of large particles in wall turbulence. Phys. Fluids 9, 3786–3807.

Patankar, N.A., 2001. A formulation of fast computations of rigid particulate flows. CTR Ann. Res. Briefs, 185–196.

Patankar, N.A., Singh, P., Joseph, D.D., Glowinski, R., Pan, T.-W., 2000. A new formulation of the distributed Lagrange multiplier/fictitious domain method for particulate flows. Int. J. Multiphase Flow, 1509–1524.

Rowe, P.N., Henwood, G.A., 1961. Drag forces in hydraulic model of a fluidised bed—Part I. Trans. Inst. Chem. Engng. 39, 43–54.

Tanaka, M., Kida, S., 1993. Characterization of vortex tubes and sheets. Phys. Fluids 5, 2079–2082.

Tsuji, Y., Morikawa, Y., Terashima, K., 1982. Fluid–dynamic interaction between two spheres. Int. J. Multiphase Flow 8, 71–82.

White, F.M., 1974. Viscous Fluid Flow. McGraw-Hill, New York.

Zhu, C., Liang, S.-C., Fan, L.-S., 1994. Particle wake effects on the drag force of an interactive particle. Int. J. Multiphase Flow 20, 117–129.